Inorganic Chemistry

Article

pubs.acs.org/IC

# Mono- and Dinuclear Manganese Carbonyls Supported by 1,8-Disubstituted (L = Py, $S_{Me}$, $S_H$) Anthracene Ligand Scaffolds

Taylor A. Manes and Michael J. Rose*

Department of Chemistry, The University of Texas at Austin, 1 University Station, A5300, Austin, Texas 78712, United States

Supporting Information

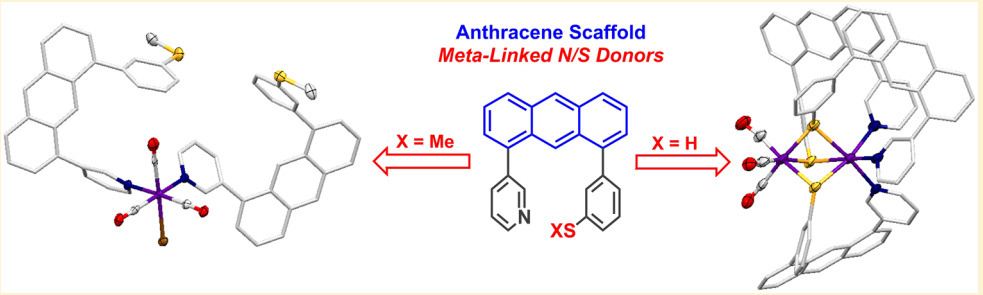


**ABSTRACT:** Presented herein is a synthetic scheme to generate symmetric and asymmetric ligands based on a 1,8-disubstituted anthracene scaffold. The metal-binding scaffolds were prepared by aryl chloride activation of 1,8-dichloroanthracene using Suzuki-type couplings facilitated by $[Pd(dba)_2]$ as a Pd source; the choice of cocatalyst (XPhos or SPhos) yielded symmetrically or asymmetrically substituted scaffolds (respectively): namely, Anth-$S_{Me}$2 (**3**), Anth-N2 (**4**), and Anth-$NS_{Me}$ (**6**). The ligands exhibit a nonplanar geometry in the solid state (X-ray), owing to steric hindrance between the anthracene scaffold and the coupled aryl units. To determine the flexibility and binding characteristics of the anthracene-based ligands, the symmetric scaffolds were complexed with $[Mn(CO)_5Br]$ to afford the mononuclear species $[(Anth\text{-}S_{Me}2)Mn(CO)_3Br]$ (**8**) and $[(Anth\text{-}N2)Mn(CO)_3Br]$ (**9**), in which the donor moieties chelate the Mn center in a cis fashion. The asymmetric ligand Anth-$NS_{Me}$ (**6**) binds preferentially through the py moieties, affording the bis-ligated complex $[(Anth\text{-}NS_{Me})_2Mn(CO)_3Br]$ (**10**), wherein the thioether-*S* donors remain unbound. Alternatively, deprotection of the thioether in **6** affords the free thiol ligand Anth-$NS_H$ (**7**), which more readily binds the Mn center. Complexation of **7** ultimately affords the mixed-valence $Mn^I/Mn^{II}$ dimer of formula $[(Anth\text{-}NS)_3Mn_2(CO)_3]$ (**11**), which exhibits a *fac*-$\{Mn(CO)_3\}$ unit supported by a triad of bridging thiolates, which are in turn ligated to a supporting Mn(II) center (EPR: $|D| = 0.053\ cm^{-1}$, $E/|D| = 0.3$, $A_{iso} = -150$ MHz). All of the metal complexes have been characterized by single-crystal X-ray diffraction, IR spectroscopy and NMR/EPR measurements—all of which demonstrate that the meta-linked, anthracene-based ligand scaffold is a viable approach for the coordination of metal carbonyls.

## INTRODUCTION

Molecular scaffolds can be a valuable tool, as they provide different binding and reactivity motifs to metal centers.[1−4] Small changes to the framework can modulate the overall binding geometry or affinity, which can then enhance or diminish the functionality of the complex. The purpose of a scaffold is to place donors or substituents in advantageous geometries to perform a designed function, and in many cases chelating ligands provide such a setting. Scaffold chelates can be classified into three groups: cis-chelating ligands,[5] wide-bite-angle ligands,[6] and trans-spanning ligands.[7,8] Scaffolding approaches can be used to enforce one or more of these ligation motifs to encourage a specific function of the metal complex. In many catalytic processes the ligand field and its arrangement around the metal center play an important role in catalytic efficiency.[9−11] Some scaffolds allow flexibility such that a complex can undergo isomerization during catalysis,[1,12] but others (such as the one we present in the current work) are more rigid and enforce a single binding geometry.

Rigid scaffolds have been used to study wide-bite and trans-chelating phosphines.[10,13] For example, a dibenzofuran system (DBFphos) was used to generate trans square-planar and tetrahedral systems. A further study by Lu et al.[4,14] installed a phenyl arm to distance the backbone from the donating phosphine atoms. This elongation prevents the furan oxygen from binding the metal center and accommodates a broader range of bite angles to allow for isomerization of intermediates, particularly in penta- and hexacoordinated catalytic systems.[14−16] Substituted anthracene scaffolds also have wide versatility in inorganic chemistry.[17] Studies have used anthracene as a trans-chelating scaffold by placing phosphines on a phenyl linker at the para position, as seen in Figure 1. The anthracene system is advantageous to trans-spanning ligands due to its aromatic frame and strategic placement of donor atoms. By using para-substituted phenyl linkers, the spacing of the donor atoms is restricted enough to allow only trans

Received: November 24, 2015

  

DOI: 10.1021/acs.inorgchem.5b02737
Inorg. Chem. XXXX, XXX, XXX−XXX

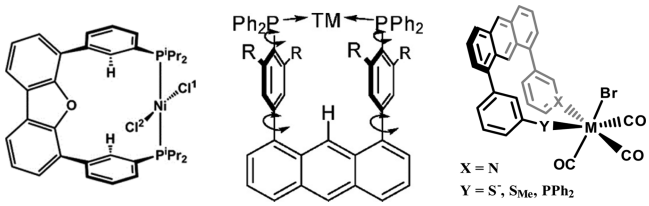


**Figure 1.** $^{ipr}$DPDBFphos[4] (left) and para-substituted anthracene[7,8] (center) scaffolds showing trans-chelated coordination environments incorporating a phenyl linker, and a model cis-chelation scaffold (right).

chelation. Trans-spanning ligands not using the scaffolding approach have been susceptible to conformational instability[18] due to their flexible nature; however, the anthracene system avoids these issues due to its rigid aromatic frame.

The anthracene model can be altered to act as a cis-chelating agent by shifting the donor linkage point to the meta position. In the present case (Figure 1, right) the donors are positioned at the meta position—in contrast to the para position used in the trans-spanning works. This conformation still retains its rigidity and stability factors; however with the donors angled inward, a cis-ligation motif should be highly favored. Another novel facet of the present system is the asymmetric nature of the donor "arms". We report a selective coupling method to incorporate both nitrogen and sulfur donors to a single ligand frame. The intent of the present work involving these cis-chelating ligands is to study their metal-binding affinity and structural aspects within the scope of a manganese(I) carbonyl environment. Mn carbonyl complexes have proven useful in catalysis, CO delivery, and detection and are common in the study of redox-active ligands.[19−23] In this work we look to evaluate and to understand the fundamental coordination chemistry of meta-linked anthracene scaffolds in the Mn environment to determine its suitability to support mononuclear metal carbonyl complexes.

## EXPERIMENTAL SECTION

**General Considerations.** All synthetic procedures were carried out under inert atmosphere ($N_2$) via Schlenk line or drybox techniques unless otherwise stated. Dry solvents were purified using a two-column alumina purification system (Pure Process Technology). Deuterated solvents were purchased from Cambridge Isotope Laboratories and used without further purification; the standard freeze−pump−thaw technique was used to degas deuterated solvents as necessary. The starting material 1,8-dichloroanthraquinone was purchased from MP Biomedicals; [Pd(dba)$_2$] (Strem), XPhos, SPhos, and 3-pyridinylboronic acid (Oakwood), (3-(methylthio)phenyl)boronic acid (Synthonix), and *tert*-nonyl mercaptan (Sigma) were purchased and used without further purification.

**Synthesis of Ligands and Synthons.** *1,8-Bis(3-(methylthio)-phenyl)anthracene, Anth-S$_{Me}$2 (**3**).* In a Schlenk flask were placed 1,8-dichloroanthracene (500 mg, 2.02 mmol), (3-(methylthio)phenyl)-boronic acid (678 mg, 4.04 mmol), and anhydrous sodium carbonate (428 mg, 4.04 mmol), and the flask was taken to the drybox. Next, [Pd(dba)$_2$] (34.8 mg, 0.0606 mmol) and XPhos (28.9 mg, 0.0606 mmol) were added to the reaction mixture. Dry THF (70 mL) was added to the reaction mixture to generate a violet solution. The reaction mixture was removed from the drybox and placed on a Schlenk line under $N_2$, at which point degassed $H_2O$ (10 mL) was added. The reaction mixture was heated to 85 °C and refluxed overnight to give a dark purple-red solution. The reaction mixture was then cooled to ambient conditions and quenched with saturated $NH_4Cl$ (5 mL), extracted with DCM (70 mL), and washed with saturated brine (2 × 100 mL). The resulting brown-yellow organic solution was dried over $Na_2SO_4$ and concentrated in vacuo to afford a brown-yellow oil. The oil was dissolved in a minimal amount of $CHCl_3$ and loaded onto a silica column packed with a 7/1 mixture of hexanes and ethyl acetate. Pure product was separated using 7/1 hexanes/ethyl acetate as eluent. The symmetric thioether ligand **3** was thus obtained as a pale yellow powder. Yield: 86% (750 mg). X-ray-quality yellow needles were grown using vapor diffusion of pentane into a solution of the complex in THF. $^1$H NMR (400 MHz, $CDCl_3$): $\delta$ 2.42 (s, 6H), 7.29 (m, 4H), 7.39 (m, 6H), 7.53 (t, 2H), 8.03 (d, 2H), 8.55 (s, 1H), 8.67 (s, 1H). $^{13}$C NMR (400 MHz CDCl3): $\delta$ 15.72, 123.52, 125.24, 125.56, 126.21, 126.71, 126.90, 127.76, 127.83, 128.49, 129.93, 131.77, 138.45, 139.97, 141.01. Selected IR frequencies (solid state, cm$^{-1}$): 3044 (w), 2917 (w), 1583 (m), 1434 (m), 872 (s). MS (CI+): *m*/*z* calcd. for $C_{28}H_{22}S_2$ (M), 422.1163; observed, 422.1169.

*1,8-Bis(pyridin-3-yl)anthracene, Anth-N2 (**4**).* In a Schlenk flask, 1,8-dichloroanthracene (500 mg, 2.02 mmol), pyridin-3-yl boronic acid (496 mg, 4.04 mmol), and anhydrous sodium carbonate (428 mg, 4.04 mmol) were added, and the flask was taken to the drybox. Next, [Pd(dba)$_2$] (34.8 mg, 0.0606 mmol) and XPhos (28.9 mg, 0.0606 mmol) were added to the reaction mixture. Dry THF (70 mL) was added to the reaction to produce a violet solution. The reaction was removed from the drybox and placed on a Schlenk line under $N_2$ where degassed $H_2O$ (10 mL) was added. The reaction was heated to 85 °C and refluxed overnight to obtain a dark purple/red solution. The reaction was cooled to ambient temperature, quenched with saturated $NH_4Cl$ (5 mL), extracted with DCM (70 mL), and washed with saturated brine (2 × 100 mL). The resulting brown/yellow organic solution was dried over $Na_2SO_4$ and concentrated in vacuo to afford a brown/yellow oil. The brown/yellow oil was dissolved in a minimal amount of $CHCl_3$ and loaded on a silica column packed with a 7:1 ratio of hexanes and ethyl acetate. Pure product was separated using MeOH as eluent. The symmetric pyridine ligand **4** was thus obtained as a dark yellow powder. Yield: 80% (536 mg). X-ray quality yellow needles were grown using vapor diffusion of pentane into a solution of the complex in THF. $^1$H NMR (400 MHz, $CDCl_3$): $\delta$ 7.35 (dd, 2H), 7.41 (d, 2H), 7.57 (dd, 2H), 7.79 (dt 2H), 8.10 (d, 2H), 8.33 (s, 1H), 8.59 (s, 1H), 8.61 (dd, 1H), 8.71 (s, 1H). $^{13}$C NMR (400 MHz, $CDCl_3$): $\delta$ 122.40, 122.90, 125.38, 126.98, 127.39, 128.57, 130.09, 131.81, 135.96, 136.57, 137.11, 148.70, 150.36. Selected IR frequencies (solid state, cm$^{-1}$): 3030 (w), 1410 (s), 1181 (s), 1023 (s), 879 (s). MS (CI+): *m*/*z* calcd for $C_{24}H_{16}N_2$ (M), 332.1313; observed, 332.1314.

*3-(8-Chloroanthracen-1-yl)pyridine, Anth-NCl (**5**).* In a Schlenk flask were placed 1,8-dichloroanthracene (500 mg, 2.02 mmol), (pyridin-3-yl)boronic acid (248 mg, 2.02 mmol), and anhydrous sodium carbonate (214 mg, 2.02 mmol), and the flask was taken to the drybox. Next, [Pd(dba)$_2$] (11.6 mg, 0.0202 mmol) and SPhos (8.3 mg, 0.0202 mmol) were added to the reaction mixture. Dry THF (70 mL) was added to generate a purple solution. The reaction mixture was removed from the drybox and placed on a Schlenk line under $N_2$, at which point $H_2O$ (10 mL) was added to the reaction mixture. The reaction mixture was heated to 85 °C and refluxed overnight to give an orange solution. The reaction mixture was cooled to ambient conditions, quenched with saturated $NH_4Cl$ (5 mL), extracted with DCM (70 mL), and washed with saturated brine (2 × 100 mL). The resulting brown-yellow organic solution was dried over $Na_2SO_4$, and concentrated in vacuo to afford a brown-yellow oil. The oil was then dissolved in a minimal amount of $CHCl_3$ and loaded onto a silica column packed with a mixture of 7/1 hexanes and ethyl acetate. Pure product was separated using 4/1 hexanes/ethyl acetate as eluent. The asymmetric precursor **5**, a yellow powder, was obtained in 37% yield (215 mg). $^1$H NMR (400 MHz, $CDCl_3$): $\delta$ 7.39 (t, 1H), 7.46 (d, 1H), 7.56 (m, 3H), 7.95 (m, 2H), 8.09 (d, 1H), 8.54 (s, 1H), 8.77 (d, 1H), 8.81 (s, 1H), 8.88 (s, 1H). $^{13}$C NMR (400 MHz, $CDCl_3$): $\delta$ 104.99, 121.81, 123.25, 125.35, 125.64, 127.28, 127.49, 127.53, 128.58, 129.21, 130.44, 132.23, 136.16, 136.87, 137.37, 148.96, 150.55. Selected IR frequencies (solid state, cm$^{-1}$): 3048 (w), 2968 (w), 2860 (w), 1615 (m), 1407 (m), 877 (s), 737 (s). MS (CI+): *m*/*z* calcd for $C_{19}H_{12}ClN$ (M), 289.0658; observed, 289.0659.


DOI: 10.1021/acs.inorgchem.5b02737
Inorg. Chem. XXXX, XXX, XXX−XXX

*3-(8-(3-(Methylthio)phenyl)anthracen-1-yl)pyridine, Anth-$NS_{Me}$ (**6**).* In a Schlenk flask were placed **5** (500 mg, 1.73 mmol), (3-(methylthio)phenyl)boronic acid (290 mg, 1.73 mmol), and anhydrous sodium carbonate (183 mg, 1.73 mmol), and the flask was taken to the drybox. Next, $[Pd(dba)_2]$ (29.8 mg, 0.051 mmol) and XPhos (24.3 mg, 0.051 mmol) were added to the reaction mixture. Dry THF (70 mL) was added to generate a purple solution. The reaction mixture was taken from the drybox and placed on a Schlenk line under $N_2$, where $H_2O$ (10 mL) was added. The reaction mixture was heated to 85 °C and refluxed overnight to afford a purple-red solution. The reaction mixture was cooled to ambient temperature, quenched with saturated $NH_4Cl$ (5 mL), extracted with DCM (70 mL), and washed with saturated brine (2 × 100 mL). The resulting brown-yellow organic solution was dried over $Na_2SO_4$, and concentrated in vacuo to afford a brown-yellow oil. The oil was dissolved in a minimal amount of $CHCl_3$ and loaded on a silica column packed with a mixture of 7/1 hexanes and ethyl acetate. Pure product was separated using 1/1 hexanes/ethyl acetate as eluent. The asymmetric ligand **6** was thus obtained as a pale yellow powder. Yield: 97% (632 mg). $^1$H NMR (400 MHz, $CDCl_3$): $\delta$ 2.46 (s, 6H), 7.24 (m, 1H), 7.39 (m, 6H), 7.55 (m, 2H), 7.82 (dt 1H), 8.07 (d, 1H), 8.08 (d, 1H), 8.49 (s, 1H), 8.57 (s, 1H), 8.62 (dd, 1H), 8.72 (s, 1H). $^{13}$C NMR (400 MHz, $CDCl_3$): $\delta$ 15.75, 122.78, 122.98, 125.16, 125.44, 125.51, 126.39, 126.65, 126.74, 127.13, 127.81, 127.85, 128.53, 128.63, 129.84, 130.15, 131.68, 131.89, 136.06, 136.60, 137.17, 138.45, 139.91, 140.87, 148.60, 150.32. Selected IR frequencies (solid state, cm$^{-1}$): 3057 (w), 2955 (w), 1584 (s), 1410 (s), 1325 (s), 1021 (s), 880 (s). MS (CI+): $m/z$ calcd for $C_{26}H_{19}NS$ (M), 377.1238; observed, 377.1241.

*3-(8-(Pyridin-3-yl)anthracen-1-yl)benzenethiol, Anth-$NS_H$ (**7**).* Under drybox conditions NaH (64 mg, 2.65 mmol) was suspended in 10 mL of DMF. Separately *tert*-nonyl mercaptan (424 mg, 2.65 mmol) was dissolved in 10 mL of DMF and then mixed with the NaH solution to produce the sodium thiolate salt and $H_2$ gas. Approximately 5 min after the mercaptan and NaH had reacted, **6** was suspended in ∼10 mL of DMF and added, generating a pink-purple solution. The Schlenk flask was then carefully taken from the drybox to the hood and placed under an $N_2$ atmosphere on a Schlenk line. The reaction mixture was set to reflux at 160 °C overnight. The resulting red-purple solution was cooled to room temperature and quenched with 4 equiv of concentrated HCl in ∼50 mL of water. The reaction mixture was manually stirred for several minutes until a flocculent yellow precipitant was observed. The precipitate was filtered over a frit and air-dried. The resulting yellow powder **7** was thus isolated in 72% yield (175 mg). $^1$H NMR (400 MHz, $CDCl_3$): $\delta$ 3.69 (b 1H), 7.29 (m, 3H), 7.42 (m, 4H), 7.55 (m, 3H), 8.07 (dd, 2H), 8.45 (s, 1H), 8.58 (s, 1H), 8.65 (dd, 1H), 8.76 (s, 1H). $^{13}$C NMR (400 MHz, $CDCl_3$): $\delta$ 123.29, 123.30, 125.56, 125.79, 126.80, 127.13, 127.50, 127.73, 128.33, 128.89, 128.95, 129.35, 130.27, 130.38, 131.00, 131.40, 132.07, 132.27, 136.46, 137.01, 137.48, 139.86, 141.55, 148.98, 150.81. Selected IR frequencies (solid state, cm$^{-1}$): 2962 (m), 2917 (m), 2871 (m), 1588 (s), 1557 (s), 1310 (s), 1032 (s), 875 (vs), 784 (vs), 747 (vs). MS (+ESI): $m/z$ calcd for $C_{25}H_{17}NS$ $(M + H)^+$, 364.1154; observed, 364.1159.

**Synthesis of Metal Complexes.** *[(Anth-$S_{Me}$2)Mn(CO)$_3$Br] (**8**).* Under drybox conditions, **3** (50 mg, 0.115 mmol) was dissolved in 10 mL of THF. Separately, $[Mn(CO)_5Br]$ (32 mg, 0.115 mmol) was dissolved in 10 mL of THF and added to the ligand solution. The dark yellow solution was stirred at room temperature overnight with no apparent color change. The solvent was removed under vacuum, resulting in dark yellow flakes. The flakes were then redissolved in a minimal amount of THF and loaded onto a short (2 mL pipet) column of neutral alumina. The complex was eluted with THF to afford **8** as a yellow powder after evacuation of solvent. Yield: 41% (30 mg). X-ray-quality yellow needles were grown using vapor effusion of a DCM solution of the complex into *n*-hexane. $^1$H NMR (400 MHz, $CDCl_3$): $\delta$ 3.01 (s, 6H), 7.35 (d, 2H), 7.48 (d, 2H), 7.53 (t, 2H), 7.60 (t, 2H), 7.75 (d, 2H), 7.81 (s, 2H), 8.10 (d, 2H), 8.45 (s, 1H), 8.62 (s, 1H). Selected IR frequencies (solid state, cm$^{-1}$): 3044 (w), 2917 (w), 2023 (vs, $\nu_{CO}$), 1933 (vs, $\nu_{CO}$), 1918 (vs, $\nu_{CO}$), 1580 (m) 879 (m), 746 (s). Anal. Calcd for $C_{31}H_{22}O_3S_2BrMn$: C, 58.04; H, 3.46; Found: C, 56.08; H, 3.35.

*[(Anth-N2)Mn(CO)$_3$Br] (**9**).* Under drybox conditions, **4** (20 mg, 0.060 mmol) was dissolved in 10 mL of THF. Separately, $[Mn(CO)_5Br]$ (16 mg, 0.060 mmol) was dissolved in THF and added to the ligand solution to generate a dark yellow solution. The reaction mixture was stirred at room temperature overnight, generating a cloudy yellow solution. The solvent was removed in vacuo to afford a yellow powder, which was redissolved into DCM and filtered over a bed of Celite to remove a flocculent suspension of solids. The yellow filtrate was concentrated in vacuo to afford an analytically pure yellow powder of **9**. Yield: 65% (22 mg). X-ray-quality yellow needles were grown using vapor effusion of a solution of the complex in DCM into *n*-hexane. $^1$H NMR (400 MHz, $CDCl_3$): $\delta$ 7.59 (b 3H), 8.03 (d, 3H), 8.28 (s, 1H), 8.59 (d, 3H), 9.10 (s, 2H), 9.51 (s, 1H), 9.80 (s, 2H), 9.93 (s, 1H). Selected IR frequencies (solid state, cm$^{-1}$): 3068 (w), 2015 (vs, $\nu_{CO}$), 1927 (vs, $\nu_{CO}$), 1888 (vs, $\nu_{CO}$), 1413 (m), 1188 (m), 737 (s). Anal. Calcd for $C_{27}H_{16}O_3N_2BrMn$: C, 58.83; H, 2.93; N, 5.08; Found: C, 58.07; H, 2.91; N, 5.00.

*[(Anth-$NS_{Me}$)$_2$Mn(CO)$_3$Br] (**10**).* Under drybox conditions, **6** (50 mg, 0.132 mmol) was dissolved in 10 mL of THF. Separately, $[Mn(CO)_5Br]$ (36 mg, 0.132 mmol) was dissolved in THF (10 mL) and added to the existing ligand solution, generating a dark yellow solution. The reaction mixture was stirred overnight with no color change. The solvent was removed in vacuo, affording a dark yellow powder. The yellow powder was redissolved in minimal THF, and loaded onto a short (2 mL pipet) column of neutral alumina. The desired product was eluted with THF to afford yellow-orange flakes. For further purification, the flakes were dissolved in fluorobenzene (10 mL) and allowed to stand overnight to produce an orange precipitate of analytically pure **10**. Yield: 32% (41 mg). X-ray-quality yellow needles were grown by layering a solution of the complex in $CHCl_3$ with pentane. $^1$H NMR (400 MHz, $CDCl_3$): $\delta$ 2.43 (s, 3H), 7.34 (d, 2H), 7.44 (d, 2H), 7.56 (t, 2H), 7.88 (d, 1H), 8.01 (d, 2H), 8.29 (s, 1H), 8.47 (s, 1H), 8.76 (d, 1H), 8.81 (s, 1H). Selected IR frequencies (solid state, cm$^{-1}$): 3060 (w), 2948 (w), 2017 (vs, $\nu_{CO}$), 1931 (vs, $\nu_{CO}$), 1900 (vs, $\nu_{CO}$), 1414 (m), 872 (s), 632 (s). Anal. Calcd for $C_{55}H_{38}O_3N_2S_2BrMn$: C, 67.83; H, 3.93; N, 2.88; Found: C, 67.86; H, 3.89; N, 2.87.

*[(Anth-NS)$_3$Mn$_2$(CO)$_3$] (**11**).* Under drybox conditions, **7** (100 mg, 0.275 mmol) was dissolved in 5 mL of THF, generating a pale yellow solution. Next, KOAc was added as a solid (27 mg, 0.275 mmol) and stirred with the ligand in solution for approximately 5 min. Finally, $[Mn(CO)_5Br]$ (75 mg, 0.275 mmol) was dissolved in 5 mL of THF. The Mn was then added, producing a darker yellow solution. As the reaction progressed, the KOAc slowly dissolved, thus facilitating deprotonation of the thiol. The reaction mixture was stirred at room temperature for 9 h, generating an orange-yellow solution not like the starting yellow solution; a copious white precipitate was also observed. The orange solution was filtered over a bed of Celite, and the solvent was removed in vacuo, producing an orange powder. The powder was washed with DCM, eliminating a yellow solution (residual $[Mn(CO)_5Br]$ and other impurities). The remaining solid was dissolved in THF and stirred with 2 equiv of $NEt_4Br$, generating another white precipitate (KBr). The solution was again filtered over Celite, affording an orange solution. The solvent was then evacuated, producing an orange-yellow powder. The yellow-orange material was dissolved in either THF or MeCN and precipitated by vapor diffusion of $Et_2O$ (>3 days), thus producing a pale yellow powder (27 mg, yield 20%). X-ray-quality yellow needles were grown using a slow vapor diffusion of $Et_2O$ into a solution of the complex in MeCN. EPR (MeCN/tol (3/1) glass, X-band, 85 K): $g$ = 2.16, $A$ = 40 G; $g$ = 2.00, $A$ = 80 G. Selected IR frequencies (solid state, cm$^{-1}$): 3044 (m), 1985 (vs, $\nu_{CO}$), 1903 (vs, $\nu_{CO}$), 1881 (vs, $\nu_{CO}$), 1550 (m), 1407 (m), 875 (m), 739 (s). Solid-state magnetic susceptibility: $\mu_{eff}$ = 5.96 $\mu_B$. FD−MS: calcd $m/z$, 1280.1619; observed $m/z$, 1281.1697.

**Physical Measurements.** $^1$H and $^{13}$C NMR spectra were collected on a Varian DirecDrive 400 MHz spectrometer, and chemical shifts ($\delta$, ppm) were referenced to the respective solvents. Infrared spectra were measured under ambient conditions on a Bruker Alpha Fourier


DOI: 10.1021/acs.inorgchem.5b02737
Inorg. Chem. XXXX, XXX, XXX−XXX

**Scheme 1. Synthetic Scheme for the Preparation of Ligands and Precursors 3−7**[a]

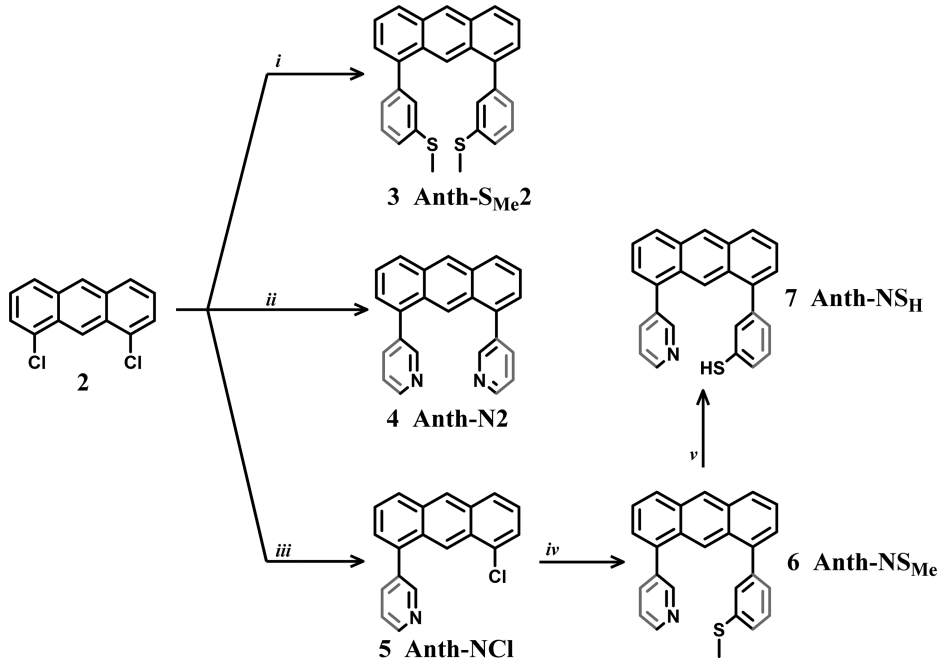


[a]Reaction conditions: (i) $Pd(dba)_2$/Xphos, $Na_2CO_3$, $THF/H_2O$ (7/1), (3-(methylthio)phenyl)boronic acid (isolated yield 86%); (ii) $Pd(dba)_2$/Xphos, $Na_2CO_3$, $THF/H_2O$ (7/1), (pyridin-3-yl)boronic acid (isolated yield 80%); (iii) $Pd(dba)_2$/Sphos, $Na_2CO_3$, $THF/H_2O$ (7/1), (pyridin-3-yl)boronic acid (isolated yield 37%); (iv) $Pd(dba)_2$/Xphos, $Na_2CO_3$, $THF/H_2O$ (7/1), (3-(methylthio)phenyl)boronic acid (isolated yield 97%); (v) *tert*-nonyl mercaptan, NaH, DMF (isolated yield 72%).

**Scheme 2. Preparation of Manganese Carbonyl Complexes**

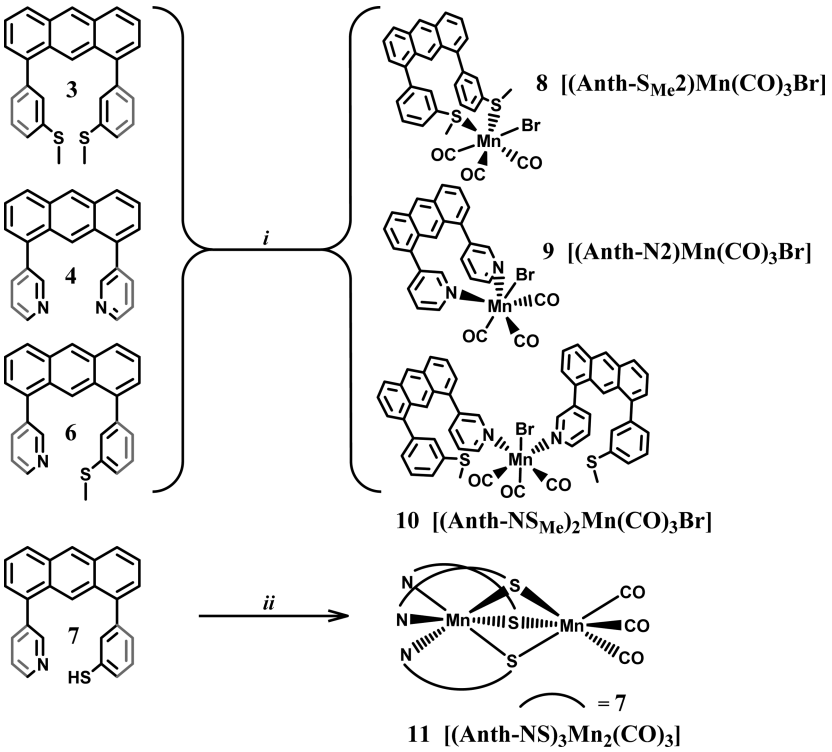


[a]Reaction conditions: (i) THF, $[Mn(CO)_5Br]$, room temperature, overnight; (ii) THF, $[Mn(CO)_5Br]$, KOAc, room temperature, 9 h.

transform infrared (FTIR) spectrometer equipped with a diamond ATR crystal. Mass spectrometry (MS) data were measured on an Agilent Technologies 6530 Accurate Mass QTofLC/MS instrument. EPR spectra were obtained with a Bruker Biospin EMXplus 114 X-band spectrometer equipped with a liquid nitrogen cryostat. The solid-state magnetic moments were determined using a Johnson-Matthey MSB Mk1 magnetic susceptibility balance. Elemental analysis was performed by Midwest Microlab LLC. Details regarding the X-ray


DOI: 10.1021/acs.inorgchem.5b02737
Inorg. Chem. XXXX, XXX, XXX−XXX

diffraction data, refinement, and instrumentation can be found in the Supporting Information. DFT calculations (Firefly software package)[24] for the dimer **11** were performed using the coordinates of the crystal structure as a starting point, with the 6-31G** basis set and the pure functional PW91.[25,26] Molecular orbitals were visualized using MacMolPlt,[27] and spin density plots were generated using gOpenMol.[28,29]

## RESULTS AND DISCUSSION

**Synthetic Rationale.** *Ligand Construction.* The synthesis of the starting material 1,8-dichloroanthracene (**2**) was performed on the basis of a hybrid of procedures previously published,[30,31] and the spectroscopic details can be found in the Supporting Information. The synthesis of the anthracene type ligands is summarized in Scheme 1 and was executed through the Suzuki cross-coupling cycle. The Suzuki cycle is catalyzed by palladium, and the functionality of the catalyst is dependent on the selected phosphine ligand. In attempts to generate ligands **3** (Anth-$S_{Me}2$) and **4** (Anth-N2), we first utilized tetrakis(triphenylphosphine)palladium(0), but we observed no reactivity of the substrates in the presence of this catalyst. On the basis of literature precedents, we also attempted reactions using alkylphosphonium salts in the presence of $[Pd(dba)_2]$, yet still observed no reactivity.[32] The use of XPhos and $[Pd(dba)_2]$ had been reported to activate aryl−chloride bonds to generate new C−C bonds between aryl halides and aryl or heterocyclic boronic acids.[33] The XPhos/$[Pd(dba)_2]$ system provided positive results with 1,8-dichloroanthracene, and as such, ligands **3** and **4** were prepared using this system. Efforts to prepare an asymmetric ligand with the XPhos/$[Pd(dba)_2]$ system demonstrated that symmetric dicoupling was preferred regardless of catalyst loading or amounts of either boronic acid. This is presumably due to the well-documented steric hindrance of the pendant $Ar(^iPr)_3$ groups near the metal site, which have been shown to accelerate the final reductive elimination step. The steric bulk present when this phosphine ligates promotes a $PdL_1$ system that is much more active than other $PdL_n$ ($n$ = 2, 4) species.[34] Thus, an alternative Pd/phosphine system was required to synthesize a suitable precursor to an asymmetric ligand.

Further screening proved that SPhos, a less sterically hindering phosphine, promoted the selective formation of the monosubstituted intermediate when reacted with 1 equiv of the (3-pyridinyl)boronic acid substituent. Anth-NCl (**5**) was thus isolated, in which a single pyridine moiety had coupled, leaving one chlorine site available for further reactivity. Upon reliable synthesis of **5**, we returned to the established XPhos system in order to couple the thioether substituent at the remaining chlorine site. Excess thioether (1.1−1.5 equiv) was used to ensure complete reaction of the chloro substituent, generating Anth-$NS_{Me}$ (**6**) in high yield. Finally, the synthesis of the free thiol ligand Anth-$NS_H$ (**7**) was achieved by deprotection of **6** with *tert*-nonyl mercaptan in DMF (160 °C).

*Complexation with Mn Carbonyl Bromide.* The propensities for coordination of the ligands were tested via complexation with the manganese(I) carbonyl source $[Mn(CO)_5Br]$. Reaction conditions can be found in Scheme 2. In the case of the bis(thioether) ligand **3**, complexation in noncoordinating solvents such as DCM proved unsuccessful. However, reactions in THF resulted in ligation of the Anth-S2 scaffold to the metal center, presumably by facilitating the loss of CO ligands promoted by the formation of intermediate THF adducts.[19] The weakly coordinating nature of THF to metal centers when in electron-deficient environments (minus a CO ligand) generates more attractive coordination conditions for the thioether moiety. Complexation of **3** afforded $[(Anth\text{-}S_{Me}2)Mn(CO)_3Br]$ (**8**) in good yield. Alternatively, the more strongly donating bis(pyridine) scaffold **4** resulted in complete formation of $[(Anth\text{-}N2)Mn(CO)_3Br]$ (**9**) in both noncoordinating and coordinating solvents (DCM and THF, respectively).

The higher affinity of the pyridine donor for the Mn(I) center is also apparent in the ligation motif of $[(Anth\text{-}NS_{Me})_2Mn(CO)_3Br)]$ (**10**), derived from the asymmetric ligand Anth-$NS_{Me}$ (**6**). Reaction of **6** with manganese carbonyl bromide was pursued in THF to accommodate the binding needs of both the pyridine and thioether donor sets. While initial results (IR, $^1$H NMR) indicated the ligation of both N and S donors, further purification by column chromatography, differential solubility, and crystallization afforded an unexpected product. Figure 4 shows the structure of **10**, wherein the thioether moieties remained unbound. The unbound thioether motif has been observed previously for Mn(I) carbonyls.[19,35] Further attempts at promoting thioether binding were performed with trimethylamine *N*-oxide (TMAO), a common decarbonylation agent. However, following addition of TMAO, complex **10** remained as the only isolable product after purification and crystallization.

*Free Thiol Ligand and Mn Complexation.* To promote sulfur binding to the Mn(I) center, the Anth-$NS_{Me}$ ligand (**6**) was modified to generate the free thiol ligand Anth-$NS_H$ (**7**). Deprotection of the thioether to generate the free thiol was achieved by reaction with *tert*-nonyl mercaptan and NaH in DMF overnight at 160 °C. The subsequent metalation of thiol **7** in THF in the presence of potassium acetate (KOAc) and the Mn(I) carbonyl for 9 h afforded an orange-yellow solution that contained primarily one product, as suggested by IR spectroscopy. Reactions for longer times—or in the presence of $NEt_4OAc$ in place of KOAc—afforded intractable mixtures of species; reactions for shorter times with KOAc afforded incomplete complexation of the Mn carbonyl starting salt, as determined by IR spectroscopy. Thus, following 9 h with KOAc, the solution was filtered and evaporated, yielding a yellow powder. The insolubility of this product in DCM or PhF suggested the formation of a charged complex. As a result, the yellow powder was washed with DCM to remove residual $[Mn(CO)_5Br]$ and uncomplexed ligand, affording the crude solid ($\nu_{CO}$ 2044, 1985, and 1890 cm$^{-1}$). Cation exchange from $K^+$ to $NEt_4^+$ using $NEt_4Br$ in THF (performed in an $N_2$-filled drybox) resulted in a complex that was more soluble in organic solvent (DCM, PhF, etc.); the complex exhibited a very similar IR spectrum ($\nu_{CO}$ 2028, 1985, and 1883 cm$^{-1}$) in the solid state, consistent with a simple counterion exchange. Subsequent crystallization in either THF or MeCN ($Et_2O$ vapor diffusion) eliminated the highest energy $\nu_{CO}$ feature (2028 cm$^{-1}$) and generated a new lower (i.e., lowest) energy feature at 1879 cm$^{-1}$. Surprisingly, X-ray analysis of the final product revealed the formula of the resulting *neutral* complex to be $[(Anth\text{-}NS)_3Mn_2(CO)_3]$ (**11**; vide infra), bearing one formally $Mn^I$ center (tricarbonyl fragment) and one oxidized $Mn^{II}$ center (with an $N_3S_3$ donor set). On the basis of the IR data, it is evident that while the $K^+ \rightarrow NEt_4^+$ exchange did not alter the composition of the initial product, extended incubation in MeCN or THF during crystallization did result in an autoredox process wherein one of the $Mn^I$ centers reduced solvent (or


DOI: 10.1021/acs.inorgchem.5b02737
Inorg. Chem. XXXX, XXX, XXX−XXX

other available moiety) to generate the mixed-valent $Mn^{I}/Mn^{II}$ final product.

**Structural Characteristics.** *Ligand X-ray Structures.* The crystal structures of Anth-$S_{Me}2$ (**3**) and Anth-N2 (**4**) (see Figures S2 and S3 in the Supporting Information, respectively) reflect their interesting 3D nature. Due to steric bulk the pyridine and aryl thioether moieties are not coplanar with the anthracene backbone. The torsion angles of the phenyl thioether moieties with respect to the anthracene scaffold are 114 and 123°, while torsion angles of the pyridine moieties are 62 and 64°. Additionally, the meta linkage of the aryl units points the N2 and $S_{Me}2$ donors away from the scaffold, maximizing the available space for binding a metal carbonyl fragment. In both cases, the donor atoms are positioned on the same side (i.e., "up−up", not "up−down") of the scaffold, thus facilitating the binding of the ligand to a single metal center. Indeed, the N atoms of the pyridine moieties of **4** appear ideally arranged for metal binding (tilted inward), whereas the S atoms of the thioether moieties in **3** (tilted outward) must overcome some steric hindrance to approach the metal site in a cis fashion. Despite these structural outcomes, it is true that we cannot be certain of the orientation of the donors in the bulk (solid) material or of the dynamic conformational flexibility in solution during complexation. X-ray-quality crystals for the unbound asymmetric ligands were not obtained despite many attempts. However, the asymmetric ligands Anth-$NS_{Me}$ (**6**) and Anth-$NS_{H}$ (**7**) can be seen in the crystal structures of the complexes [(Anth-$NS_{Me}$)$_2$Mn(CO)$_3$Br] (**10**) and [(Anth-NS)$_3$Mn$_2$(CO)$_3$] (**11**) (Figures 4 and 5), the details of which are discussed below.

*Structures of Metal Complexes.* The structures of complexes [(Anth-$S_{Me}2$)Mn(CO)$_3$Br] (**8**) and [(Anth-N2)-Mn(CO)$_3$Br] (**9**) (Figures 2 and 3, respectively) both exhibit

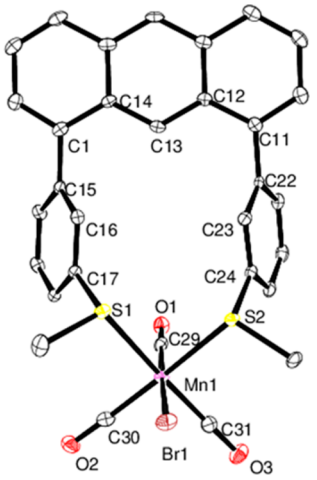


**Figure 2.** ORTEP diagram (30% ellipsoids) of [(Anth-$S_{Me}2$)Mn-(CO)$_3$Br] (**8**) with the labeling scheme. H atoms are omitted for clarity.

ligation of the bidentate ligand in a cis fashion to a {Mn(CO)$_3$Br} fragment. The bite angle between the thioether-*S* donors in **8** is 83.63°, contributing to the pseudo-octahedral coordination environment. Analogously, the bite angle between the pyridine-*N* donors in **9** is 90.38°, contributing to a nearly ideal octahedral shape. Both cases demonstrate that the combination of ligand flexibility and donor spacing promotes facile metal binding. As a result of the

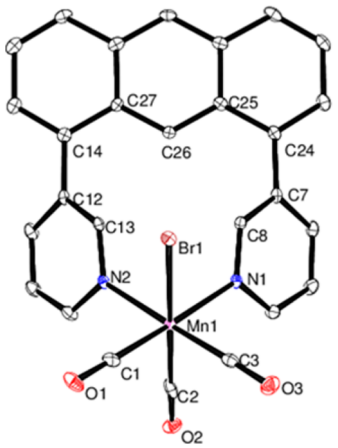


**Figure 3.** ORTEP diagram (30% ellipsoids) of [(Anth-N2)Mn-(CO)$_3$Br] (**9**) with the labeling scheme. H atoms are omitted for clarity.

cis-binding motif, each Mn center binds the three CO ligands in a facial orientation, with the orthogonal face composed of the two ligand donors and halide. Interestingly, in the case of **8**, the metal core buckles underneath the ligand, somewhat occupying the vacancy between the two aryl linkers. This is attributable to the steric influence effect of the thioether $CH_3$ groups—both directed "upward" in **8**. The Mn−S bond distances of 2.3903(13) and 2.3850(13) Å are slightly longer than those reported for previous Mn(I) thioether carbonyls, such as 2.3001(8)[19] and 2.362(2) Å.[36] A decrease in the torsion angle associated with the Mn complex is also observed, as the free rotation is restricted by the Mn center. Angles decrease from ∼115° in the free ligand to 57° in the metal complex. The remaining distances of interest may be found in Table 1.

**Table 1. Selected Bond Distances (Å), Bond Angles (deg), and Torsion Angles (deg) for [(Anth-$S_{Me}2$)Mn(CO)$_3$Br] (8), [(Anth-N2)Mn(CO)$_3$Br] (9), and [(Anth-$NS_{Me}$)$_2$Mn(CO)$_3$Br] (10)**[a]

| | 8 | 9 | 10 |
|---|---|---|---|
| Mn−$N_1$ | | 2.135(3) | 2.102(4) |
| Mn−$N_2$ | | 2.139(3) | 2.093(4) |
| Mn−$S_1$ | 2.3903(13) | | |
| Mn−$S_2$ | 2.3850(13) | | |
| Mn−C(O) | 1.800(5) | 1.818(4) | 1.917(7) |
| | 1.817(5) | 1.837(4) | 1.813(5) |
| | 1.800(5) | 1.800(4) | 1.816(5) |
| $N_1$−Mn−$N_2$ | | 90.38(10) | 84.86(15) |
| $S_1$−Mn−$S_2$ | 83.63(5) | | |
| Mn−Br | 2.5069(8) | 2.5217(6) | 2.5329(9) |
| torsion | 57.6(6) | 45.8(4) | 74.4(6) (py) |
| | | | 114.5(5) ($S^{Me}$) |

[a]Torsion angles were measured using the ortho and peri carbons of the anthracene and respective substituents.

Similar to the case for **8**, complex **9** exhibits a cis chelation motif of the bis(pyridine) ligand **4** to the {Mn(CO)$_3$Br} fragment. As a result, the facial arrangement of CO ligands is analogous to that in **8**, and the Mn−C and Mn−Br bond distances are quite similar (Table 1). The pyridine arms in **8** are twisted from planarity with respect to the anthracene plane (torsion angle 45.8(4)°). Upon inspection of the torsion angles


DOI: 10.1021/acs.inorgchem.5b02737
Inorg. Chem. XXXX, XXX, XXX−XXX

in the unbound ligand **4** (torsion angle 62.0(3)°), it is apparent that the presence of the Mn center in **8** is responsible for the further twisting of the pyridine moieties toward the anthracene plane. As a result, in the presence of the Mn ion, the proximal ortho C−$H_{py}$ units at the "top" of the pyridine are in close contact in complex **8** (H···H = 2.19 Å), versus the much longer H···H contact of 3.54 Å in unbound ligand **4**. It is notable that both values are still greater than the sum of the van der Waals radii of the H atoms (2.18 Å), suggesting at least a minimal extent of steric clash in the case of the Mn complex.

While we were unable to grow crystals of the asymmetric ligand **6** (Anth-$NS_{Me}$), we did obtain crystals of its corresponding metal complex, $[(Anth\text{-}NS_{Me})_2Mn(CO)_3Br]$ (**10**), depicted in Figure 4. The most notable feature of the

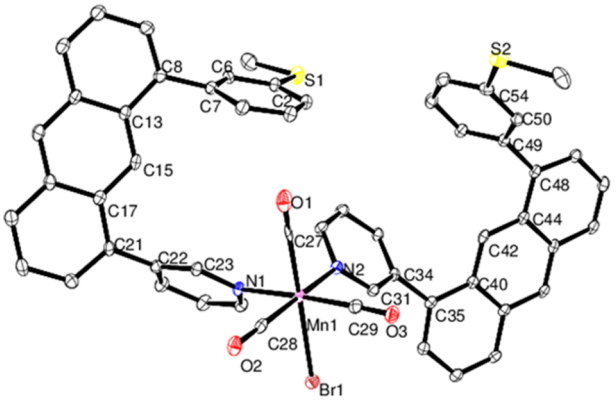


**Figure 4.** ORTEP diagram (30% ellipsoids) of $[(Anth\text{-}NS_{Me})_2Mn(CO)_3Br]$ (**10**) with the labeling scheme. H atoms are omitted for clarity.

complex is that two ligands bind a single manganese center via their nitrogen donors. The thioether moiety on each ligand remained unbound, at an approximate distance of ∼8.43 Å from the metal center. The higher affinity of pyridine-*N* versus the thioether-*S* for the Mn(I) center is thus suggested by this structure, as described in Synthetic Rationale. Interestingly, the Mn−$N_{py}$ bonds in **10** (2.102(4), 2.093(4) Å) are slightly shorter than the Mn−$N_{py}$ bonds in **9** (2.135(3), 2.139(3) Å), suggesting that the steric effects of the bis(pyridine) chelate **4** prevent complete encroachment of the $N_{py}$ donors in **9** to the metal center. Additionally, despite the fact that there are two separate ligands (no chelate effect), and considering the steric implications, the pyridine moieties are still bound close to each other in a cis fashion. This is likely attributable to the propensity of the manganese tricarbonyl moiety to retain its "piano stool" configuration, vis à vis the preference of strongly back-bonding CO ligands to bind trans to stronger σ donors.

The lack of binding between the thioether-*S* and Mn(I) center prompted us to explore the ligation properties of the mixed pyridine/thiolate ligand Anth-$NS_H$ (**7**). The resulting structure of $[(Anth\text{-}NS)_3Mn_2(CO)_3]$ (**11**) is shown in Figure 5, which reveals two manganese centers ligated by three pyridine/thiolate chelates. During the synthesis, isolation, and crystallization of the complex, the presence of the more nucleophilic thiolate had two primary effects: (i) the *intended* effect of promoting both N and S binding and (ii) the *unintended* effect of promoting a redox event at one of the manganese centers (despite isolation/crystallization under an inert atmosphere). The result is that one metal center is oxidized to a Mn(II) that binds all three $N_{py}$ donors, while the other remains a Mn(I)

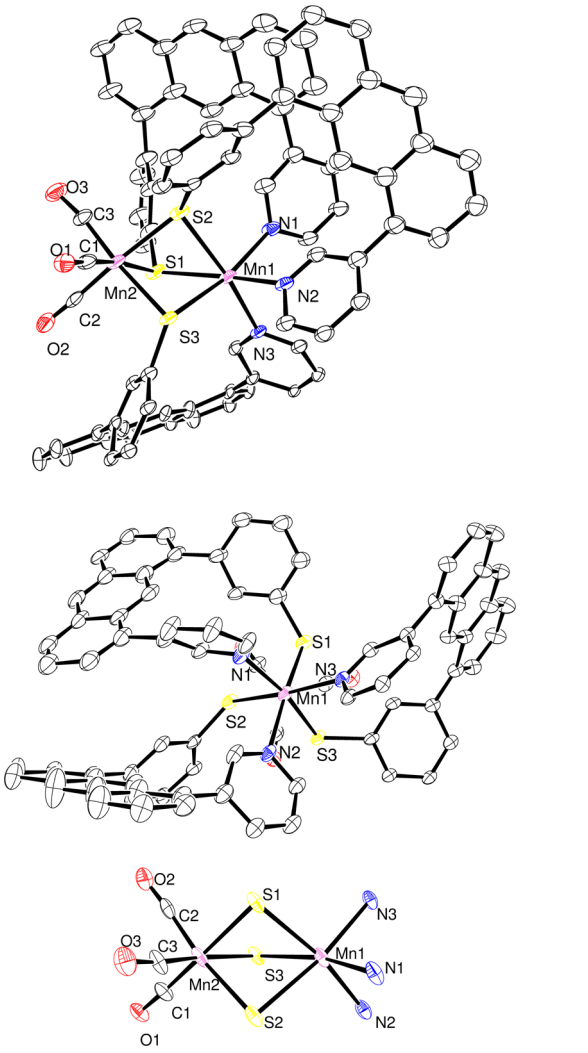


**Figure 5.** Three views of the ORTEP diagram (30% ellipsoids) of $[(Anth\text{-}NS)_3Mn_2(CO)_3]$ (**11**) with the labeling scheme. The "axial" view (middle view) shows the "asymmetric" orientation of the anthracene moieties about the dimer "core". The "core" view (bottom view) eliminates the anthracene scaffolds and is depicted for visual clarity. In the top view, H atoms are omitted for clarity, while the bottom view excludes all ligand-based C and H atoms. *Note:* in the bottom view $N_1/S_1$, $N_2/S_2$, and $N_3/S_3$ are the chelate pairings.

center that retains its CO ligands; the Mn(I) and Mn(II) centers are bridged by the three $\mu_2$-S thiolate bridges. Further evidence for the $Mn^I$−$Mn^{II}$ dimer is provided in Spectroscopy, and selected bond distances and angles may be found in Table 2. Overall, the ligation motif exhibited by complex **11** demonstrates a successful attempt to bis-ligate a metal center with an asymmetric anthracene-based scaffold in a cis orientation. However, further work will be required to extend the series of mononuclear complexes by sterically preventing dimerization across the thiolato-*S* donor(s) and adjacent metals.

**Spectroscopy.** *Infrared Spectra.* Figure 6 depicts the infrared spectrum obtained for each Mn complex. Considering only the donor atoms ligated directly to the metal center, the complexes $[(Anth\text{-}S_{Me}2)Mn(CO)_3Br]$ (**8**), $[(Anth\text{-}N2)Mn(CO)_3Br]$ (**9**), and $[(Anth\text{-}NS_{Me})_2Mn(CO)_3Br]$ (**10**) have approximate $C_s$ symmetry. Evaluation of the appropriate character tables predicts each complex should exhibit three


DOI: 10.1021/acs.inorgchem.5b02737
Inorg. Chem. XXXX, XXX, XXX−XXX

**Table 2. Selected Bond Distances (Å) and Bond Angles (deg) for $[(Anth\text{-}NS)_3Mn_2(CO)_3]$ (11) and Calculated Bond Distances and Bond Angles from the $S = {}^5/_2$ DFT-Optimized Structure**

| | 11 | calcd |
|---|---|---|
| $Mn_1–N_1$ | 2.269(10) | 2.321 |
| $Mn_1–N_2$ | 2.310(11) | 2.285 |
| $Mn_1–N_3$ | 2.282(8) | 2.329 |
| $Mn_1–S_1$ | 2.600(4) | 2.553 |
| $Mn_1–S_2$ | 2.651(3) | 2.601 |
| $Mn_1–S_3$ | 2.610(3) | 2.556 |
| $Mn_2–S_1$ | 2.426(3) | 2.469 |
| $Mn_2–S_2$ | 2.411(4) | 2.450 |
| $Mn_2–S_3$ | 2.403(3) | 2.448 |
| $Mn_2–CO$ | 1.768(12) | 1.767 |
| | 1.777(15) | 1.765 |
| | 1.771(12) | 1.761 |
| $N_1–Mn_1–S_1$ | 103.2(3) | 98.89 |
| $N_2–Mn_1–S_2$ | 98.9(2) | 103.17 |
| $N_3–Mn_1–S_3$ | 103.2(2) | 103.21 |

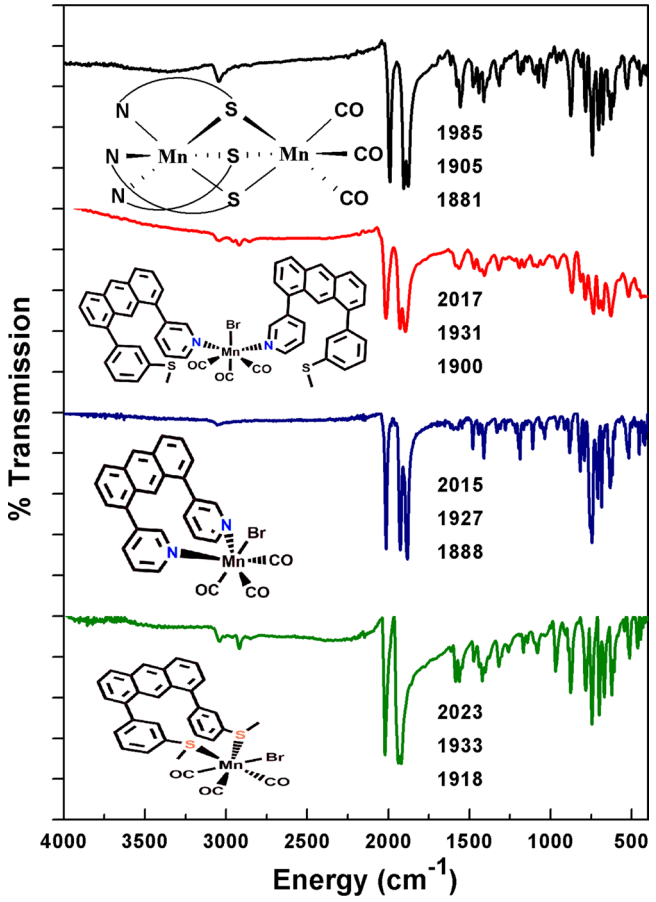


**Figure 6.** Infrared spectra of **8** (bottom green trace), **9** (middle blue trace), **10** (middle red trace), and **11** (top black trace) showing carbonyl stretches associated with each complex.

carbonyl stretches. As seen in Figure 8, indeed all three exhibit such properties. Complex **8** exhibits CO stretches at 2023, 1933, and 1918 $cm^{-1}$, complex **9** exhibits CO stretches at 2015, 1927, and 1888 $cm^{-1}$, and complex **10** exhibits CO stretches at 2017, 1931, and 1900 $cm^{-1}$. Each of these complexes has a CO stretch above 2000 $cm^{-1}$, which could be most closely associated with a CO trans to the halide. The other two stretches seen in each complex are observed as two sharp features in close proximity in the vicinity of 1910 ± 20 $cm^{-1}$.

On the other hand, $[(Anth\text{-}NS)_3Mn_2(CO)_3]$ (**11**) has approximate $C_{3v}$ symmetry (again considering only the symmetry of the metal centers plus donor atoms). In this case, the group theory evaluation suggests that only two stretches should be visible in the IR spectra. However, the spectrum of a crystalline sample of **11** reveals three carbonyl stretches overall occurring at 1985, 1905, and 1881 $cm^{-1}$. First, it is notable that the highest $\nu$(CO) value in **11** (1985 $cm^{-1}$) is lower than the highest $\nu$(CO) values in **8**–**10**. This is attributable to the stronger $\sigma$-donor strength of the three thiolato-*S* donors bound in a position trans to the *fac*-$\{Mn(CO)\}^+$ fragment. However, as described in Structural Characteristics, the three thiolato-*S* donors are not crystallographically equivalent. As noted above, the mixed $Mn^I$–$Mn^{II}$ oxidation state system incurs a disparity in $Mn_1–S_x$ bond distances into two sets: two short bonds and one long bond. The IR data suggest that the inequivalent Mn–S bonding motifs lower the predicted symmetry of the molecule from $C_{3v}$ to $C_s$, thus affording similar absorption spectra to complexes **8**–**10**. Additionally, it is notable that the crystalline solid, powder, and solution IR spectra of **11** (Figure S21 in the Supporting Information) all exhibit the higher energy feature (1990, 1985, 1985 $cm^{-1}$, respectively) and the lower energy feature(s) (1903 and 1878 $cm^{-1}$, sharp; 1892 $cm^{-1}$, broad; 1899 $cm^{-1}$, broad; respectively), strongly suggesting that the structure observed in the crystal structure is retained in solution. Indeed, **11** can be dissolved in noncoordinating solvent ($CH_2Cl_2$, PhF) or coordinating solvent (THF) and reisolated as the pure complex by either solvent evaporation or recrystallization; no loss of CO or other change in composition is observed. Furthermore, the FD-MS (gentle ionization method) of **11** reveals a peak (M + H) at $m/z$ 1281.1697 (Figure S22 in the Supporting Information), consistent with the calculated mass of $m/z$ 1280.1619. There is no evidence to suggest that the structure of **11** in solution is different from that in the crystal.

*Electron Paramagnetic Resonance (EPR) and Magnetism.* Regarding the thiolate-based complex $[(Anth\text{-}NS)_3Mn_2(CO)_3]$ (**11**), the charge-balance, lack of observable features in the $^1H$ NMR spectrum, and differential bond metrics led us to hypothesize the presence of a paramagnetic Mn(II) center in the complex. As the structure clearly indicates discrete $\{Mn(CO)_3\}$ and $\{Mn(N3)(S3)\}$ moieties, it was reasonable to hypothesize a mixed-valence dimer containing the well-known Mn(I) tricarbonyl "piano stool" moiety and a distinct (and localized) Mn(II) center bound by the remaining heteroatoms. As such, we pursued EPR studies of the complex—both in the solid state and in solution.

The solid-state EPR spectrum of polycrystalline **11** over a range of temperatures (288–88 K) is shown in Figure 7. Unlike the case for the solution phase, the primary features can be observed at both room temperature and at 88 K, although the $^{55}Mn$ hyperfine features are not resolved at any temperature. The spectrum exhibits a primary feature at $g = 2.02$, which itself could be consistent with either an $S = 1/2$ or an $S = 5/2$ system.[37,38] However, the four additional features at both lower fields ($g = 5.56$, 2.86) and higher fields ($g = 1.50$, 1.22) are *inconsistent* with an $S = 1/2$ system but *consistent* with an $S = 5/2$ Kramers manifold. To provide further evidence for the $S = 5/2$ configuration for the Mn(II) ion in **11**, we pursued simulations of the data (EasySpin;[39] CW solid state module).


DOI: 10.1021/acs.inorgchem.5b02737
Inorg. Chem. XXXX, XXX, XXX–XXX

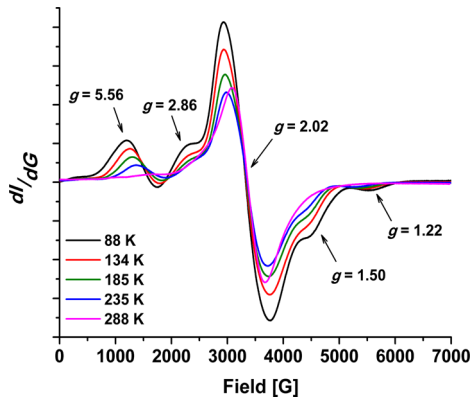


**Figure 7.** Solid-state powder EPR spectra of $[(Anth\text{-}NS)_3Mn_2(CO)_3]$ (**11**) acquired in the range of 88−288 K, with prominent features labeled with the associated $g$ values. Instrument parameters: $\nu$ = 9.43 GHz, modulation frequency 100 kHz, modulation amplitude 8 G, microwave power 2 mW.

As shown in Figure 8, an excellent agreement between simulation (top) and experiment (bottom, 88 K) was obtained

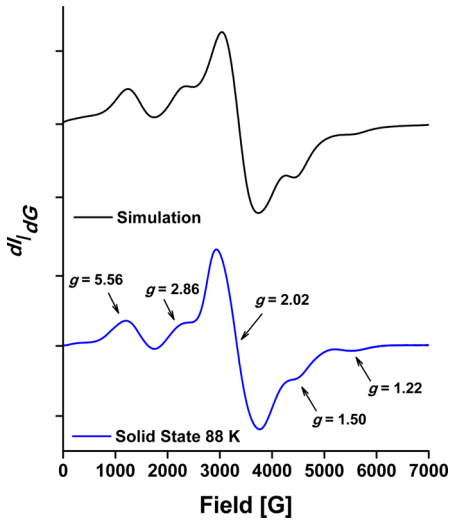


**Figure 8.** Simulated (top) and experimental (bottom, 88 K) solid-state EPR spectra for $[(Anth\text{-}NS)_3Mn_2(CO)_3]$ (**11**). Prominent features are labeled with the associated $g$-values. Simulation parameters: $S$ = 5/2; $E/|D|$ = 0.3; $|D|$ = 0.053 $cm^{-1}$; isotropic $^{55}Mn$ hyperfine $A_{iso}$ = −150 MHz; line broadening (Lorentzian/Gaussian) 32/16.

using a $g$ tensor of 2.0. High-spin Mn(II) (or any high-spin $d^5$) complexes exhibit spherical electron density about the metal center and therefore generally have small Zeeman interactions; this leads to $g$ values near 2.0.[40] Indeed, DFT spin density calculations (Figure 10) reveal the expected spherical spin density around the $Mn^{2+}$ center.

Regarding the zero field splitting (ZFS), the simulated EPR spectrum utilized $|D|$ = 0.053 $cm^{-1}$ and $E/|D|$ = 0.30. As discussed in a review by Neese and co-workers,[40] octahedral Mn(II) complexes without halides exhibit very small ZFS parameters ($|D| \approx$ 0.01−0.1 $cm^{-1}$). Although thiolate donors were not considered in that review, the bridging nature of the thiolates in **11**, coupled with their covalent character, renders them more akin to oxygen donors than halides. Indeed, the majority of six-coordinate Mn(II) complexes with mixed N/O ligation exhibit $|D| \approx$ 0.01−0.1 $cm^{-1}$. Much higher $|D|$ values (0.1−1 $cm^{-1}$) are only associated with lower coordination numbers and/or the presence of halides. The best-fit $E/|D|$ ratio of 0.30 in the simulation was indicative of a predominantly rhombic system. Indeed, despite the seemingly symmetric $N_3S_3$ donor set (apparently axial coordination environment), closer inspection of the bond distances (Table 2) coincide with the rhombic interpretation. In the structure of **11** (Figure 5), the display of supporting anthracene moieties is *not* in the arrangement of a $C_3$ "propeller": while two anthracene units are aligned in counterclockwise fashion, the third orients in a clockwise orientation. This arrangement of anthracene moieties translates into the first coordination sphere, wherein there are two similar Mn−N bonds (2.269(10), 2.282(8) Å) and one distinct Mn−N bond (2.310(11) Å); the same trend is observed for the Mn−S bonds (2.600(4) and 2.610(3) Å versus 2.651(3) Å). Thus, the local asymmetry of the $N_3S_3$ coordination sphere appears sufficient to induce rhombic character in the system.

Solutions of **11** (3/1 MeCN/toluene) at room temperature afforded no observable features; however, frozen glasses at 85 K afforded the spectrum shown in Figure 9. The primary feature

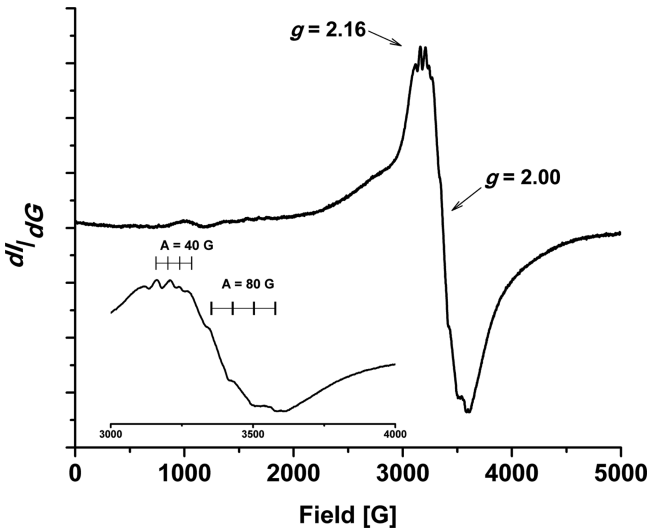


**Figure 9.** EPR spectrum of $[(Anth\text{-}NS)_3Mn_2(CO)_3]$ (**11**) obtained at 85 K in a frozen glass of 3/1 MeCN/toluene. Inset: expanded view of the primary feature in which the hyperfine coupling is observed. Instrument parameters: $T$ = 85 K, $\nu$ = 9.43 GHz, modulation frequency 100 kHz, modulation amplitude 8 G, microwave power 2 mW.

of the broad spectrum is centered near $g \approx$ 2.00.[37,38] In this solution spectrum, the metal-centered nature of the unpaired electron is apparent in the two sets of hyperfine features due to the $I$ = 5/2 $^{55}Mn$ nucleus. More specifically, there is one set of hyperfine features near $g$ = 2.1 (40 G), as well as a distinct set of broader hyperfine features near $g$ = 2.0 (80 G). Such nuclear hyperfine is not observed in the solid-state sample due to the close proximity of Mn centers in the solid state (faster relaxation times) in comparison to the dilute solution (1 mM). It is also notable that the minor features observed in the solid-state spectrum at higher field ($g$ = 5.56, 2.86) are somewhat masked by the broadness of the solution spectrum. Importantly, the simulated EPR spectrum (Figure S23 in the Supporting Information) using $A_{iso}$ = −150 MHz (−50 × $10^{-4}$ $cm^{-1}$) along with drastically diminished line broadening exhibited independent sets of hyperfine features near $g$ = 2.1 (45 G) and $g$ =


DOI: 10.1021/acs.inorgchem.5b02737
Inorg. Chem. XXXX, XXX, XXX−XXX

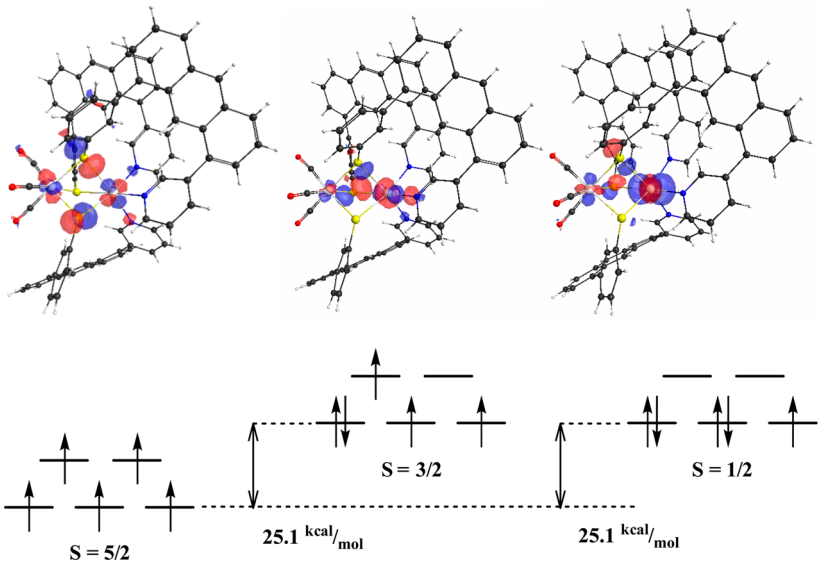


**Figure 10.** DFT calculated energies of the $S$ = 5/2, 3/2, and 1/2 configurations using the X-ray coordinates of **11** (6-31G**/PW91). The highest energy SOMO in each case is shown above its respective configuration.

2.0 (60 G). Such an $A_{iso}$ value ($-50 \times 10^{-4}$ cm$^{-1}$) is consistent with those compiled by Neese and co-workers ($|A_{iso}| \approx (68-100) \times 10^{-4}$ cm$^{-1}$).[40] Overall, these data—coupled with observations that the IR spectrum in solution closely matches that of the solid-state IR (vide supra)—suggests that the connectivity of **11** determined by X-ray diffraction is largely retained in solution.

The solid-state magnetic properties of **11** were also investigated. The magnetic susceptibility of **11** at 298 K was determined to be $\mu_{eff}$ = 5.96 $\mu_B$, quite close to the predicted spin-only value for an $S$ = 5/2 system ($\mu_{SO}$ = 5.92). Thus, the consistent EPR behavior in both solution and the solid state, as well as the solid state $\mu_{eff}$ value, suggests that Mn(II) ion in the dimer exists in all cases in the $S$ = 5/2 configuration. This conclusion was further supported by DFT calculations (next section).

**Density Functional Theory (DFT).** The dimeric structure of $[(Anth\text{-}NS)_3Mn_2(CO)_3]$ (**11**) was examined by DFT calculations to determine the lowest energy spin multiplicity of the complex (Figure 10). To this end, spin multiplicity calculations were performed on the unoptimized X-ray coordinates of **11**, under the presumption of $S$ = 1/2, 3/2, and 5/2 configurations. Although the $S$ = 3/2 calculation did not converge as readily $S$ = 1/2 and $S$ = 5/2 calculations, the high-spin $S$ = 5/2 configuration was found to be roughly 25.1 kcal/mol more stable than the lower spin states. This result is consistent with the experimentally determined magnetic susceptibility value of 5.96 $\mu_B$. After this unequivocal result was obtained, optimization of the coordinates in the $S$ = 5/2 case afforded very good to excellent agreement with the bond distances and angles derived from X-ray analysis (see Table 2). Indeed, closer inspection of the bond distances surrounding the $\{Mn(N_3)(S_3)\}$ unit reveal bond metrics—especially the Mn−N bonds—more closely associated with high-spin versus low-spin systems. The Mn−N bond lengths of 2.269(10), 2.310(11), and 2.282(8) Å found in the dimer **11** are similar to those in other reported high-spin systems (e.g., Mn−N = 2.2499(16) Å)[41] and are much longer than those in reported low-spin systems (e.g., Mn−N = 2.003(2) Å).[42]

To confirm that the spin density was indeed localized on the formally manganese(II) $\{Mn(N_3)(S_3)\}$ unit, a spin density plot was generated from the DFT calculations (Figure 11). The

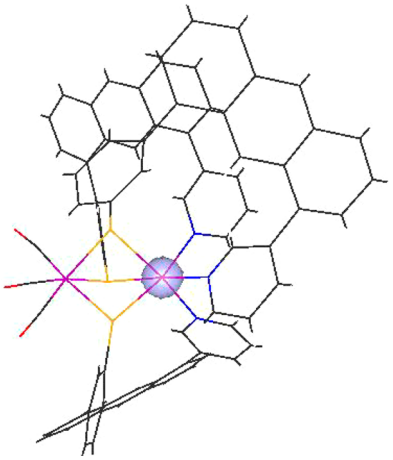

**Figure 11.** DFT calculated spin density plot for the geometry optimized structure of **11** (6-31G**/PW91).

strong localization of the spin on the Mn(II) center is isotropic, as a result of the evenly distributed spin across the five d orbitals. We also analyzed the DFT calculated nuclear charges, which were found to be quite distinct for the two Mn centers. Both the calculated Mulliken charges (0.825 versus 0.274) and Lowdin charges (0.164 versus −0.527) clearly indicate discrete oxidation states for the $\{Mn(N_3)(S_3)\}$ ion and the $\{Mn(CO)_3\}$ ion, respectively. On the basis of all of the DFT results, we can conclude the dimer **11** is a mixed-valence system best described as a class I system, where there is no delocalization of spin or charge, and also no observable IVCT band.

## CONCLUSION

We have demonstrated the design and synthesis of anthracene ligand scaffolds bearing meta-linked aryl moieties for metal binding. Previous work by others described trans ligation using anthracene scaffolds with para-linked aryl donors, but by


DOI: 10.1021/acs.inorgchem.5b02737
Inorg. Chem. XXXX, XXX, XXX−XXX

shifting the donors to the meta positon, the cis-ligation motif was favored. We also report for the first time a synthetic method for the synthesis of asymmetric anthracene scaffolds. The cis ligation by both symmetric and asymmetric ligands was observed in both monometallic and bimetallic complexes, the latter of which was supported by a mixed pyridine/thiolate ligand. The mixed pyridine/thiolate ligand afforded the mixed-valence dimer **11**, which includes a localized high-spin Mn(II) ion as determined by solution EPR, solid EPR, magnetic moments, and DFT calculations. In future endeavors, similar anthracene chelators will be implemented with iron(II) carbonyl species to pursue facially coordinating, small-molecule mimics of mono-[Fe] hydrogenase—an ongoing topic of research in our laboratory. Additional studies will be performed to discern if the anthracene scaffold approach can achieve both structural and functional modeling of this natural organometallic complex.

## ■ ASSOCIATED CONTENT

### Supporting Information

The Supporting Information is available free of charge on the ACS Publications website at DOI: 10.1021/acs.inorgchem.5b02737.

Crystallographic data (CIF)

Complete X-ray data tables, $^{1}H$ and $^{13}C$ NMR spectra, and mass spectral characterizations of ligands and complexes (PDF)

## ■ AUTHOR INFORMATION


### Corresponding Author

*E-mail for M.J.R.: mrose@cm.utexas.edu.


### Notes

The authors declare no competing financial interest.

## ■ ACKNOWLEDGMENTS

This research was supported by the Robert A. Welch Foundation (F-1822), and the ACS Petroleum Research Fund (53542-DN13). The authors thank Dr. Vince Lynch for assistance with X-ray data collection and the refinement of structures, and we thank Dr. Kory Mueller for aiding in the collection of EPR spectra. We also acknowledge Zhu-Lin "Sam" Xie for assistance in performing DFT calculations.

## ■ REFERENCES


(1) Birkholz, M.-N.; Freixa, Z.; van Leeuwen, P. W. N. M. *Chem. Soc. Rev.* **2009**, *38*, 1099−1118.

(2) Freixa, Z.; van Leeuwen, P. W. N. M. *Coord. Chem. Rev.* **2008**, *252*, 1755−1786.

(3) Freixa, Z.; van Leeuwen, P. W. N. M. *Dalt. Trans.* **2003**, 1890−1901.

(4) Marlier, E. E.; Tereniak, S. J.; Ding, K.; Mulliken, J. E.; Lu, C. C. *Inorg. Chem.* **2011**, *50*, 9290−9299.

(5) Elsevier, C. J.; Reedijk, J.; Walton, P. H.; Ward, M. D. *Dalton Trans.* **2003**, 1869−1880.

(6) van Leeuwen, P. W. N. M.; Kamer, P. C. J.; Reek, J. N. H. *Pure Appl. Chem.* **1999**, *71*, 1443−1452.

(7) Kaganovsky, L.; Cho, K.; Gelman, D. *Organometallics* **2008**, *27*, 5139−5145.

(8) Bessel, C. A.; Aggarwal, P.; Marschilok, A. C.; Takeuchi, K. J. *Chem. Rev.* **2001**, *101*, 1031−1066.

(9) Kaganovsky, L.; Gelman, D.; Rueck-Braun, K. *J. Organomet. Chem.* **2010**, *695*, 260−266.

(10) Kranenburg, M.; van der Burgt, Y.; Kamer, P.; van Leeuwen, P. W. *Organometallics* **1995**, *14*, 3081−3089.

(11) Kamer, P. C. J.; Van Leeuwen, P. W. N. M.; Reek, J. N. H. *Acc. Chem. Res.* **2001**, *34*, 895−904.

(12) Hamann, B. C.; Hartwig, J. F. *J. Am. Chem. Soc.* **1998**, *120*, 3694−3703.

(13) Haenel, M. W.; Jakubik, D.; Rothenberger, E.; Schroth, G. *Chem. Ber.* **1991**, *124*, 1705−1710.

(14) Ding, K.; Miller, D. L.; Young, V. G.; Lu, C. C. *Inorg. Chem.* **2011**, *50*, 2545−2552.

(15) Jiménez-Rodríguez, C.; Roca, F. X.; Bo, C.; Benet-Buchholz, J.; Escudero-Adán, E. C.; Freixa, Z.; van Leeuwen, P. W. N. M. *Dalton Trans.* **2006**, 268−278.

(16) Fairlamb, I. J. S.; Grant, S.; Tommasi, S.; Lynam, J. M.; Bandini, M.; Hao, D.; Zhenyang, L.; Whitwood, A. C. *Adv. Synth. Catal.* **2006**, *348*, 2515−2530.

(17) Lamm, J. H.; Vishnevskiy, Y. V.; Ziemann, E.; Kinder, T. a.; Neumann, B.; Stammler, H. G.; Mitzel, N. W. *Eur. J. Inorg. Chem.* **2014**, *2014*, 941−947.

(18) Smith, R. C.; Protasiewicz, J. D. *Organometallics* **2004**, *23*, 4215−4222.

(19) Lumsden, S. E.; Durgaprasad, G.; Thomas Muthiah, K.; Rose, M. J. *Dalton Trans.* **2014**, *43*, 10725−10738.

(20) Rimmer, R. D.; Pierri, A. E.; Ford, P. C. *Coord. Chem. Rev.* **2012**, *256*, 1509−1519.

(21) Hartl, F.; Rosa, P.; Ricard, L.; Le Floch, P.; Záliš, S. *Coord. Chem. Rev.* **2007**, *251*, 557−576.

(22) Deeming, A. J.; Karim, M.; Bates, P. A.; Hursthouse, M. B. *Polyhedron* **1988**, *7*, 1401−1403.

(23) Begum, N.; Hyder, M. I.; Kabir, S. E.; Hossain, G. M. G.; Nordlander, E.; Rokhsana, D.; Rosenberg, E. *Inorg. Chem.* **2005**, *44*, 9887−9894.

(24) Granovsky, A.. http://classic.chem.msu.su/gran/gamess/index.html.

(25) Perdew, J. P.; Chevary, J. A.; Vosko, S. H.; Jackson, K. A.; Pederson, M. R.; Singh, D. J.; Fiolhais, C. *Phys. Rev. B: Condens. Matter Mater. Phys.* **1993**, *48*, 4978.

(26) Perdew, J. P.; Chevary, J. A.; Vosko, S. H.; Jackson, K. A.; Pederson, M. R.; Singh, D. J.; Fiolhais, C. *Phys. Rev. B: Condens. Matter Mater. Phys.* **1992**, *46*, 6671−6687.

(27) Bode, B. M.; Gordon, M. S. *J. Mol. Graphics Modell.* **1998**, *16*, 133−138.

(28) Laaksonen, L. *J. Mol. Graphics* **1992**, *10*, 33−34.

(29) Bergman, D. L.; Laaksonen, L.; Laaksonen, A. *J. Mol. Graphics Modell.* **1997**, *15*, 301−306.

(30) Goichi, M.; Segawa, K.; Suzuki, S.; Toyota, S. *Synthesis* **2005**, 2116−2118.

(31) Pérez-Trujillo, M.; Maestre, I.; Jaime, C.; Alvarez-Larena, A.; Piniella, J. F.; Virgili, A. *Tetrahedron: Asymmetry* **2005**, *16*, 3084−3093.

(32) Dai, C.; Fu, G. C. *J. Am. Chem. Soc.* **2001**, *123*, 2719−2724.

(33) Martin, R.; Buchwald, S. L. *Acc. Chem. Res.* **2008**, *41*, 1461−1473.

(34) Christmann, U.; Vilar, R. *Angew. Chem., Int. Ed.* **2005**, *44*, 366−374.

(35) Gonzalez, M. A.; Carrington, S. J.; Fry, N. L.; Martinez, J. L.; Mascharak, P. K. *Inorg. Chem.* **2012**, *51*, 11930−11940.

(36) Connolly, J.; Goodban, G. W.; Reid, G.; Slawin, A. M. Z. *J. Chem. Soc., Dalton Trans.* **1998**, 2225−2232.

(37) Pike, R. D.; Rieger, A. L.; Rieger, P. H. *J. Chem. Soc., Faraday Trans. 1* **1989**, *85*, 3913−3925.

(38) Tao, L.; Stich, T. A.; Butterfield, C. N.; Romano, C. A.; Spiro, T. G.; Tebo, B. M.; Casey, W. H.; Britt, R. D. *J. Am. Chem. Soc.* **2015**, *137*, 10563−10575.

(39) Stoll, S.; Schweiger, A. *J. Magn. Reson.* **2006**, *178*, 42−55.

(40) Duboc, C.; Collomb, M. N.; Neese, F. *Appl. Magn. Reson.* **2010**, *37*, 229−245.

(41) Walesa-Chorab, M.; Kubicki, M.; Korabik, M.; Patroniak, V. *Dalt. Trans* **2013**, *42*, 9746−9754.




DOI: 10.1021/acs.inorgchem.5b02737
*Inorg. Chem.* XXXX, XXX, XXX−XXX

(42) Saha, A.; Majumdar, P.; Goswami, S. *J. Chem. Soc. Dalt. Trans.* **2000**, 1703−1708.



DOI: 10.1021/acs.inorgchem.5b02737
*Inorg. Chem.* XXXX, XXX, XXX−XXX